Pathoconnectomics of neurodegeneration

Bryan William Jones, Rebecca Pfeiffer, Crystal Sigulinsky, James Anderson
Moran Eye Center, University of Utah School of Medicine

Abstract: Ultrastructural connectomics approaches have given us new insight into the precise wiring topologies of neural circuits mediating fundamentals of mammalian vision, critical to normal functioning. Pathoconnectomics is simply the application of volume EM or ultrastructural connectomics approaches to disease tissues. These pioneering approaches have given us insight into the very earliest features of neural degenerative disease that have revised our assumptions about how neurodegeneration progresses. We assumed that neurodegenerative disease would proceed in a chaotic fashion, and we were wrong. The earliest stages of neurodegeneration feature predictable, stereotyped alterations in neuronal and glial morphology, connectivity, protein expression, and function revealing the neural circuit topology behind the earliest clinical sequelae of neurodegeneration. Earlier explorations of a retinal model of neurodegeneration suggested changes in pharmacological response, as well as metabolic alterations in the content of Müller glia, and bipolar cell populations. Hybridizing metabolomics with ultrastructural connectomics and pathoconnectomics approaches revealed the source of metabolic and proteomic alterations in both glia and bipolar cell neurons engaged in the earliest stages of retinal degeneration. In short, bipolar cell populations in mammalian retina come in 3 classes present in roughly equal proportions, ON-cone, OFF, and rod bipolar cells. In normal tissues, only ON-cone bipolar cells are coupled via gap junctions to Aii amacrine cells and the glycine content in them derives from that coupling. In early retinal degeneration all bipolar cell classes begin expressing connexins and couple with Aii amacrine cells at specific locations, revealing potential clinical intervention points.

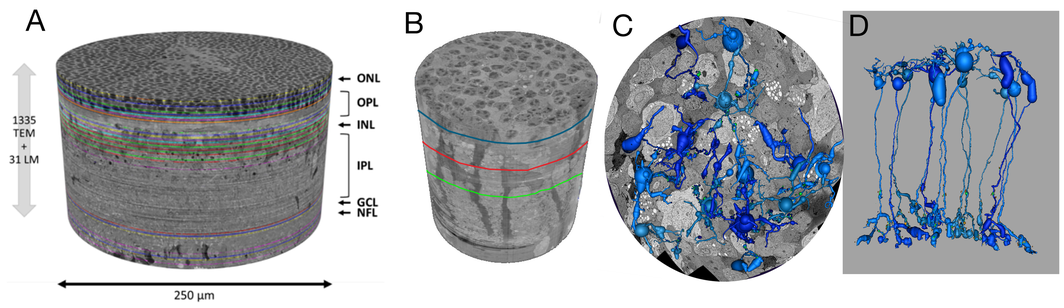

Figure 1 Retinal Connectomes and Pathoconnectomes: A. Exemplar normal retinal connectome (RC1, RC2, RC3), captured with transmission electron microscopy at 2nm/pixel. RC1 = normal rabbit retina, RC2 = normal mouse retina, RC3 = normal non-human primate retina. **B.** Exemplar retinal pathoconnectomes (RPC1, RPC2, RPC3). The existing RPCs are all of rabbit retina using a transgenic model of autosomal dominant retinitis pigmentosa. Future retinal pathoconnectomes in non-human primate retina are underway for models of AMD, optic neuropathy, and achromatopsia. **C.** Retinal Pathoconnectome 1 (RPC1) overlay of a top down view of the 3D renderings of all confirmed 16 rod bipolar cells (RodBCs) and cone-contacting rod bipolar cells (XRodBCs) in the RPC1 volume on a representative TEM section from RPC1. **D.** Vertical view of the 3D reconstruction of RodBC and XRodBCs in RPC1.

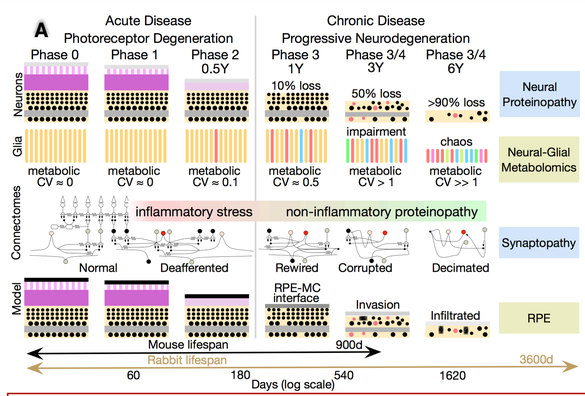

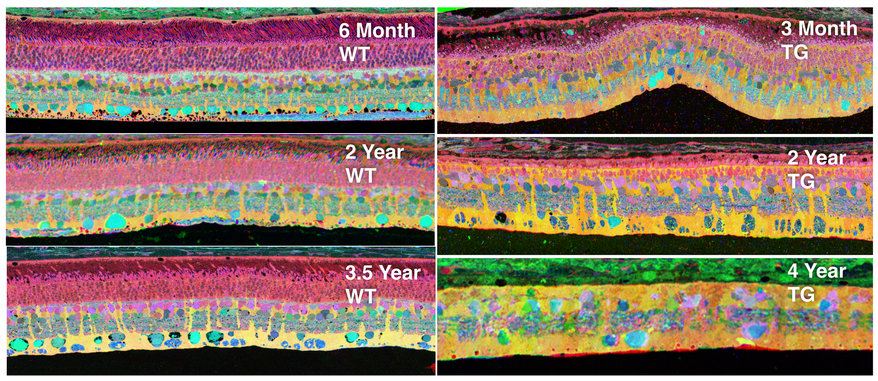

Figure 2 Retinal Degeneration: **A** Retinal degeneration is a phased revision of the normal circuitry and topology of the retina. Retinal degeneration and remodeling encompasses cell death, rewiring, metabolic and protein alterations. **B** Representative taurine (τ), glutamine (Q), and glutamate (E) (rgb,respectively) labeled sections from healthy WT retina vs. degenerate retina from P347L transgenic rabbits. Throughout aging the WT retinas τQE signtaures and anatomical structure remain relatively constant. In the P347L trangenic animal (**C**), the retina progressively denegerates with age. Variability in metabolic signature between Müller cells can be seeen as early as 3 months degeneration and persists as the animal ages and the retina continues to degenerate. Anatomically, by 2 yrs of age, outer photoreceptor segments have degenerated; by 4 yrs, photoreceptors have been entirely lost.

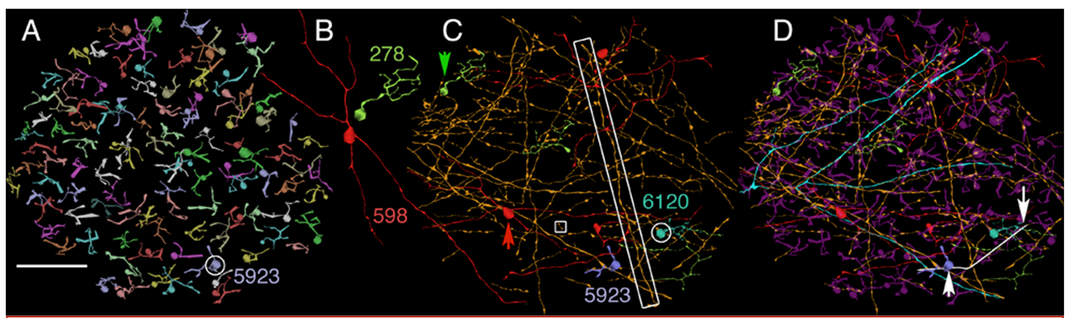

Figure 3 RC1 bipolar and amacrine annotations. A. Renderings of all rod BC axon terminals in retinal connectome 1 (RC1), captured with transmission electron microscopy at 2nm/pixel. Rod BC 5923 is circled. Each different color is a single rod BC terminal. **B.** Wide-field γAC 598 (red) and narrow-field GAC 278 (green). **C.** A field of γAC (orange) and GAC (green) processes, γAC 598 (red, up arrow) and GAC 278 (green, down arrow) that provide cross-channel inhibition to every rod BC encountered. ON cone CBb5 6120 is circled. The smallest and largest inhibitory distances mediated by γACs are shown in the square and rectangle, respectively. **D.** The inhibitory field of processes superimposed on the rod BC field (magenta). Motif C1 γAC process 32477 (white process, arrows) spans rod BC 5923 and CBb5 6120. Scale 0.1 mm for A,C,D and 69 µm for B.

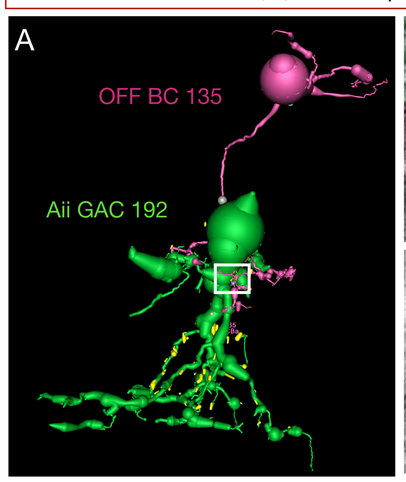

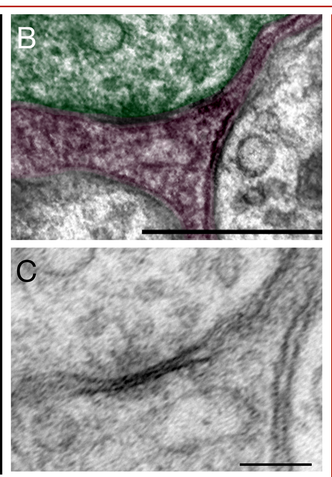

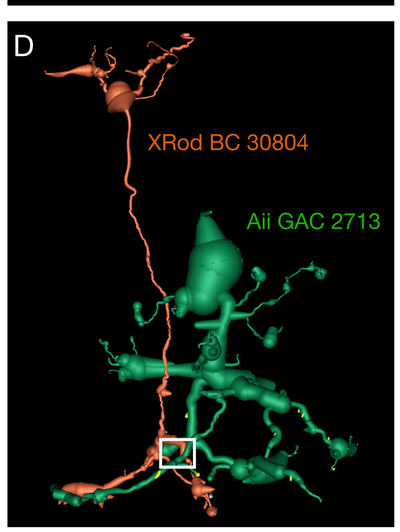

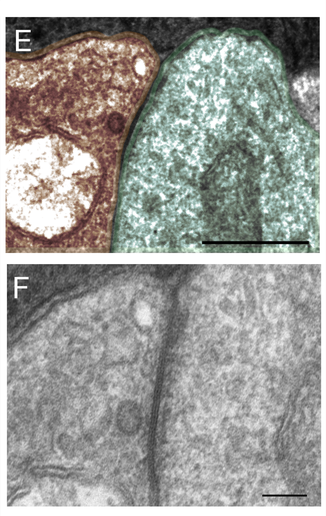

Figure 4 Aberrant synaptology in RPC1 Off Bipolar Cells and Rod Bipolar cells: A. 3D rendering of OFF bipolar cell 135 (pink) and Aii glycinergic amacrine cell 192 (green). **B.** Pseudocolored TEM image of region indicated by box in A. demonstrating gap junctional connection between OFF bipolar cell 135 and Aii glycinergic amacrine cell 192. Scale bar = 200nm. **C.** Higher magnification of gap junction shown in B. recaptured at 25,000x (.436nm/px) tilted to -10 degrees. Scale bar = 100nm. **D.** 3D rendering of an indeterminate rod bipolar cell 30804. This rod bipolar cell receives synaptic contacts from rod photoreceptor cells, but also receives synaptic inputs from cone photoreceptors. Yet it laminates in the plexiform layer associated with rod bipolar cells. **E.** Pseudocolored TEM image of region indicated by box in D. demonstrating gap junctional connection between XRod Bipolar Cell 30804 and Aii glycinergic amacrine cell 2713. Scale bar = 200nm. **F.** Higher magnification of gap junction shown in D recaptured at 25,000x (.436nm/px) tilted to +5 degrees showing the pentalaminar structure associated with gap junctions. Scale bar = 100nm.

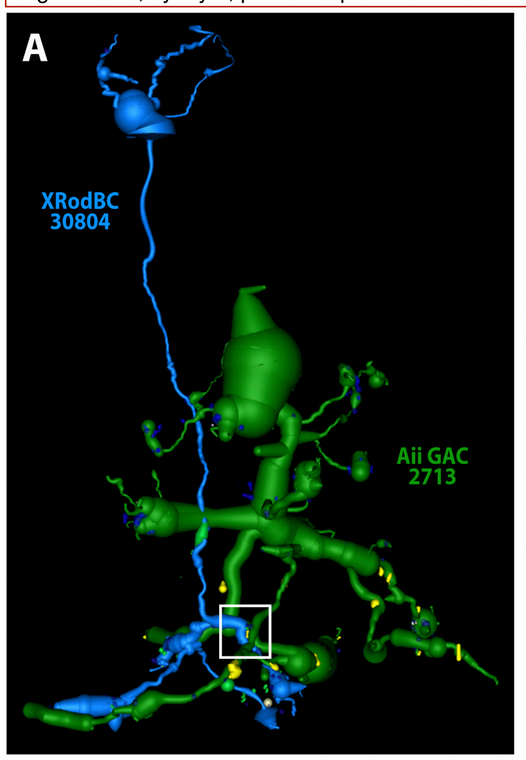

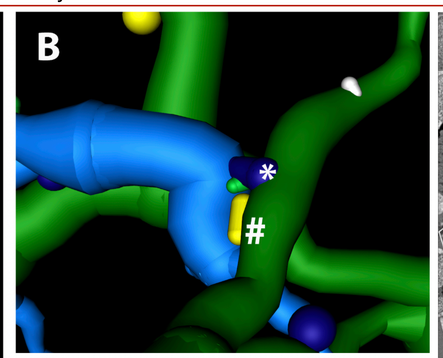

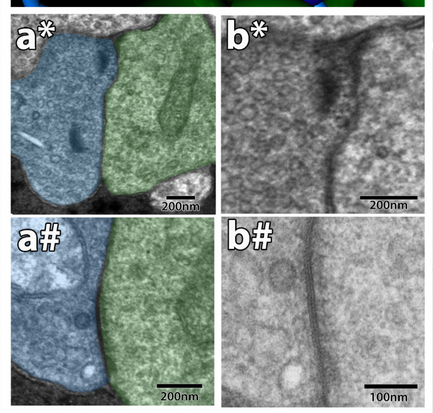

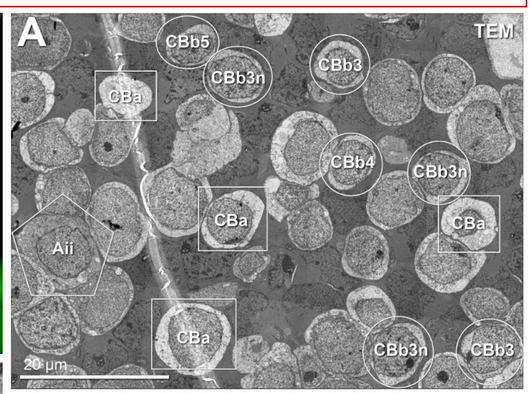

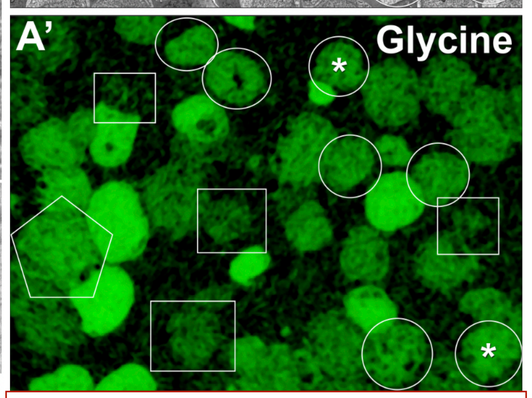

Figure 6 Glycine co-localization: Circles = ON cone bipolar cells. Rectangles = OFF cone bipolar cells. Pentagon = Aii amacrine cell.

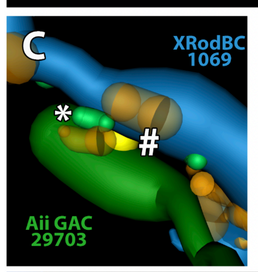

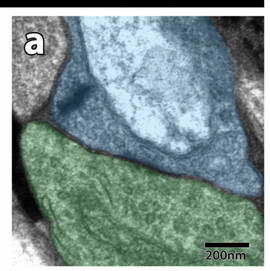

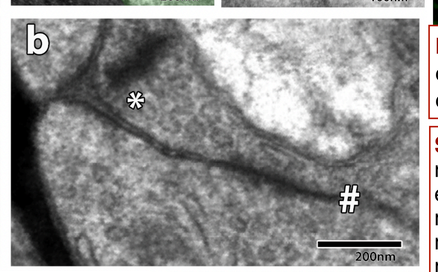

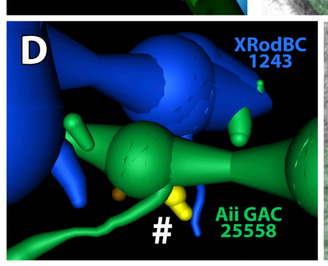

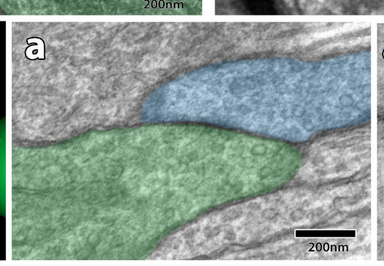

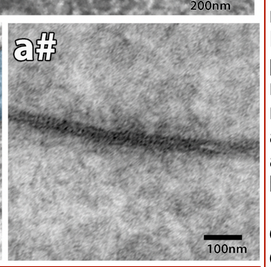

Figure 5 Abberant synaptology in RPC1: (A) 3D rendering of XRodBC 30804 (blue) and Aii GAC 2713 (green). (B) Higher magnification of region indicated by box in A. * indicates a glutamatergic ribbon and # indicates a gap junction between the XRodBC and Aii GAC (a*) Pseudo-colored TEM image of the ribbon indicated in B. (b*) Higher magnification of ribbon indicated in B. (a#) Pseudo-colored TEM image of gap junction indicated in B. (b#) Recaptured TEM image at 25k (.436nm/px) tilted to -5 degrees. (C) 3D rendering of gap junction and ribbon annotations between XRodBC 1069(blue) and Aii GAC 29703 (dark green). (a) Pseudo-colored TEM image of ribbon and gap junction in C. (b) Higher magnification TEM image of ribbon (*) and gap junction (#) in C. (d) 3D rendering of gap junction annotation between XRodBC 1243(blue) and Aii GAC 25558 (dark green). (a) Pseudo-colored TEM image of gap junction in d. (a#) Recaptured TEM image at .436nm/px tilted to -10 degrees.

Summary: Aii amacrine cells bridge input from the rod photoreceptors mediating scotopic light to the evolutionarily older cone photoreceptor system that mediates transmission of photopic light levels. In normal mammalian retinas ON cone bipolar cells make gap junctions with Aii amacrine cells. However, in early retinal degeneration, prior to photoreceptor cell loss, a series of phased revisions happens that alters the circuit topology of retina. Glutamate receptor expression becomes altered (data not shown), followed by metabolic alterations in both glia (see Figure 2 above) and in bipolar cell populations (data shown above). Protein expression profiles in rod and OFF bipolar cell populations is then altered and those cell classes make inappropriate gap junctional connections with Aii glycinergic amacrine cells.

Contact:
bryan.jones@m.cc.utah.edu
@BWJones / @bwjones.bsky.social
http://prometheus.med.utah.edu/~bwjones/

Funding:
Grants NIH EY02576, EY015128, EY014800, NSF 2014862, and an unrestricted grant from Research to Prevent Blindness to the Moran Eye Center, an unrestricted grant from Gabe Newell to BWJones.